IEEE Access
Multidisciplinary | Rapid Review | Open Access Journal

Received February 4, 2020, accepted February 14, 2020, date of publication February 18, 2020, date of current version March 3, 2020.

Digital Object Identifier 10.1109/ACCESS.2020.2974913

A Convex Variational Approach for Image Deblurring With Multiplicative Structured Noise

TINGTING WU[1], WEI LI[1], LIHUA LI[2], AND TIEYONG ZENG[3]

[1]School of Science, Nanjing University of Posts and Telecommunications, Nanjing 210023, China
[2]College of Life Information Science and Instrument Engineering, Hangzhou Dianzi University, Hangzhou 310018, China
[3]Department of Mathematics, The Chinese University of Hong Kong, Hong Kong

Corresponding author: Tieyong Zeng (zeng@math.cuhk.edu.hk)

This work was supported in part by the Natural Science Foundation of China under Grant 61971234, Grant 11501301, Grant 11671002, Grant 61731008, and Grant U1809205, in part by The Chinese University of Hong Kong (CUHK) Start-Up and CUHK Direct Grant for Research under Grant 4053296, Grant 4053342, Grant RGC 14300219, and Grant NSFC/RGC N_CUHK 415/19, and in part by the 1311 Talent Plan of Nanjing University of Posts and Telecommunications (NUPT).

ABSTRACT The restoration of images corrupted by blurring and structured noise has attracted growing attention in the domains of image processing and computer vision. However, many works only focus on the restoration of the images degraded by blurring and additive structured noise or multiplicative structured noise separately. It is still a challenge and an open problem to restore degraded images with blurring and multiplicative structured noise, simultaneously. In this paper, based on the total variation (TV), the statistical property of the Gamma noise and the maximum a posteriori (MAP) estimator, we obtain a convex variational model to recover blurred images with multiplicative structured noise. Especially, to get this convex model, we reformulate the prior assumption of the images degradation model by division instead of multiplication. For solving this convex model, an effective alternating direction method of multipliers (ADMM) is employed. Numerical experiments are presented to illustrate the effectiveness and efficiency of the proposed model.

INDEX TERMS Image deblurring, convex variational model, structured noise, multiplicative noise, ADMM.

I. INTRODUCTION

Image deblurring and denoising are fundamental tasks in image processing and computer version. In real applications, image blurring is unavoidable due to many factors such as long transmission distance, environmental electromagnetic interference, and air turbulence [1]. Moreover, the observed images can be further affected by both blurring and noise interference in the process of image acquisition and transmission [2], [3]. Generally, we can consider two kinds of random noises: additive and multiplicative noise. Under the additive noise scheme, numerous deblurring methods have been proposed to handle these problems. We refer the readers to see [4]–[15]. Indeed, various regularization approaches (e.g. the wavelet frame [5], [14], [15] and the total variation (TV) [4], [6], [7], [11]) were used to recover good numerical results from the additive noise. Under the multiplicative noise scheme, the blurred image Hu was further corrupted by some multiplicative noise η. The degradation model is as follows,

$$u_0 = Hu \odot \eta, \tag{1}$$

where $u \in \mathbb{R}^{m\times n}$ is the original image; H is the blurring operator and u_0 is the observed image; and $\eta \in \mathbb{R}^{m\times n}$ is a random vector that could follow one or more statistical distributions such as Gamma distribution and Gaussian distribution. Let E denote the vector space of 2D images defined on $\Omega = \{1, \ldots, m\} \times \{1, \ldots, n\}$. For any 2D images, the total number of pixels is $m \times n$. The pixels of the image are identified by a multi-index $i = (i_1, i_2) \in \Omega$. The point-wise product between two elements Hu and η is denoted $Hu \odot \eta$,

$$(Hu \odot \eta)[i] = (Hu)[i]\eta[i]. \tag{2}$$

Unlike the additive noise with independent properties, multiplicative noise is generally coupled with the original images. Though this standard multiplicative noise assumption can model some real applications such as synthetic aperture radar (SAR), ultrasound imaging, and laser images [16], it still lost many image information seriously, especially the structural

The associate editor coordinating the review of this manuscript and approving it for publication was Emanuele Crisostomi.

information. In coherent imaging systems, the photographs that we observed have distinct structural features. For instance, we could observe the ripple effect in X-ray imaging [17], [18], the speckle noise in ultrasonic imaging [19]–[21], and the stripes effect in medical equipment imaging [22]. In this paper, we mainly consider the restoration of blurred images under multiplicative structured noise. To the best of our knowledge, this problem has not yet been studied. To take the structure information into account, similarly to [23], [24], we use a stationary noise η to replace the standard assumption describing the structural information of the noise. We can generate the structured noise η by convolving the noise ν with a known kernel,

$$\eta = \psi \star \nu, \tag{3}$$

where the operator ψ is a convolution filter that depends on the noise structure, the symbol $\star$ is the convolution product, and the convolution product $\eta = \psi \star \nu$ is defined by

$$\eta[i] = \sum_{j\in\Omega} \psi[i-j]\nu[j], \tag{4}$$

where the noise ν is a random vector. It can be seen that structured noise η depends on the structure ψ and the noise ν.

Until the past decade, a few variational methods have been proposed to handle the problem of images degraded by blurring and multiplicative noise. When the blur operator $H = Id$ in (1) (i.e. Id is an identity operator), these problems become the multiplicative noise removal problems. Rudin *et al.* [25] firstly proposed the variation model to solve this issue (called "RLO model"),

$$\begin{aligned} &\min_u \|u\|_{TV}, \\ &\text{s.t.} \sum_{i=1}^{mn} \frac{[u_0]_i}{[u]_i} = 1, \\ &\sum_{i=1}^{mn} \left(\frac{[u_0]_i}{[u]_i} - 1\right)^2 = \sigma^2, \end{aligned} \tag{5}$$

where σ^2 is the noise variance, and $\|u\|_{TV}$ is the total variation of u to preserve the shape edges (see Section II-A for details). The RLO model only uses the basic statistical properties, the mean and the variance, which limits the image restoration effect. Based on the Gamma noise with the mean of 1, Aubert and Aujol [26] used a maximum a posteriori (MAP) estimator to obtain a multiplicative denoising model (called "AA model"),

$$\min_u \|u\|_{TV} + \alpha \sum_{i=1}^{mn} \left(\log[u]_i + \frac{[u_0]_i}{[u]_i}\right), \tag{6}$$

where α is a parameter that balances the data fidelity term and the TV term. Although the AA model is non-convex, Aubert and Aujol proved that the objective equation has an optimal solution. The non-convexity of the RLO and AA model poses serious numerical troubles. Shi and Osher [27] proposed a globally convex total variational framework (called "SO model"). They transformed the multiplicative noise into the additive noise through logarithmic transformation and used the spatial method to remove multiplicative noise. Huang *et al.* [28] maintained the framework of the AA model by using a transformation $w = \log u$, this model is strictly convex and the alternating direction method of multipliers (ADMM) was proposed to find the optimal solution of the objective function. The numerical results show that the restoration effect of this method is better than the AA model. Steidl and Teuber [29] proposed a convex variational model based on I-divergences to recover images corrupted by multiplicative noise. Dong *et al.* [30] proposed the nonlocal total variational model to restore multiplicative noise and used the split Bregman method to deal with this minimization problem. Inspired by the Gaussian adaptive method for denoising, Chen and Cheng [31] developed a multiplier denoising model with local constraints of TV regularization term, which can automatically select regular parameters by using the statistical properties of random variables. Except for TV regularization methods, there are also many other ways to remove multiplicative noise well such as dictionary learning, tight-frame approach and so on. We refer the reader to see [32]–[39].

In recent years, many scholars have investigated the problem of image deblurring with multiplicative noise. The classical RLO and AA model can be extended to restore blurred images,

$$\begin{aligned} &\min_u \|u\|_{TV}, \\ &\text{s.t.} \sum_{i=1}^{mn} \frac{[u_0]_i}{[Hu]_i} = 1, \\ &\sum_{i=1}^{mn} \left(\frac{[u_0]_i}{[Hu]_i} - 1\right)^2 = \sigma^2, \end{aligned} \tag{7}$$

and

$$\min_u \|u\|_{TV} + \alpha \sum_{i=1}^{mn} \left(\log[Hu]_i + \frac{[u_0]_i}{[Hu]_i}\right). \tag{8}$$

To overcome the drawback of the non-convex model in (7) and (8), Dong and Zeng [40] proposed a convex denoising and deblurring model by introducing a quadratic penalty term into the AA model. In [41], Wang and Ng transformed the multiplicative noise and blur removal problem into the additive denoising and deblurring problem by logarithmic transformation and used the ADMM algorithm to solve it. Dong and Zeng [42] used an I-divergence technique to build a convex model. Zhao *et al.* [43] proposed a model containing the total variational regular term, the data fidelity term, and the variance term, and obtained analytical solutions by ADMM algorithm. Shama *et al.* [44] proposed a convex model, which contains the data fidelity term based on MAP, the penalty term based on total generalized variational regularization and noise statistical characteristics, separately. There are also other models and algorithms focusing on this topic [7], [16], [45]–[52].

In order to get higher quality images, the problem of restoring images with structured noise has been getting more and more attention in the fields of space, biological sciences, and medical imaging. Münch *et al.* [53] combined the wavelet and Fourier transform to remove stripes and ring artifacts. Boas and Fleischmann [54] summarized the algorithms and restoration models for recovering computed tomography (CT) imaging. Henrik Fitschen *et al.* [55] used a variational model with directional first and second order differences to recover stripes noise. Roels *et al.* [56] analyzed the main factors of image degradation and proposed a non-local means image restoration algorithm to restore images under the 3D electron microscope. Chen *et al.* [57] proposed a method based on TV regularization and group sparsity constraint to deal with the fringe noise of remote sensing images. Fehrenbach *et al.* [24] (see Section II-B for details) proposed a variational stationary noise removal method to remove the additive structured noise in the scanning electron microscope. In [23], the authors proposed a variational model based on Gamma distribution to restore multiplicative structured noise (see Section II-C for details). This model is convex and provides good recovering results. Han et al. proposed a novel algorithm based on a new definition of similarity coefficient to remove PolSAR image speckle [58]. Yang et al. used the Schatten 1/2-norm regularization to the remote sensing images destriping [59]. However, all of the above methods only focus on the restoration of the images degraded by blurring and additive structured noise or multiplicative structured noise separately. As far as we know, it is still a challenge and an open problem to restore degraded images with blurring and multiplicative structured noise, simultaneously.

In this paper, inspired by the pioneer works [23], [24], we study the deblurring issues with multiplicative structured noise. Comparing with previous works, our contributions are as follows.

- First, we propose a convex variational model to restore the images degraded by blurring and multiplicative structured noise.
- Second, we adopt the standard ADMM algorithm to solve the proposed model, and this algorithm has a better effect and speed.
- Third, numerical experiments show that our model and algorithm have good numerical performance and are very robust in recovering images under different blur kernels, different types of structured noise and different Gamma noise levels.

The rest of this paper is organized as follows. In Section 2, we review the total variation regularization and the related works of [23], [24]. We propose our model to restore blurred images with multiplicative structured noise in Section 3. In Section 4, the ADMM algorithm is employed to solve the proposed model. In Section 5, we demonstrate the effectiveness and efficiency of the proposed model by some numerical experiments. Conclusions are drawn in Section 6.

II. RELATED WORKS

A. TOTAL VARIATION REGULARIZATION

In [60], Rudin et al. firstly introduced the total variation $\|u\|_{TV}$ in image restoration to preserve sharp edges. The discrete total variation of u can be defined by [16]

$$\begin{aligned}\|u\|_{TV} &= \sum_{1\le j\le m,1\le k\le n} \left|(\nabla u)_{j,k}\right|_2 \\ &= \sum_{1\le j\le m,1\le k\le n} \sqrt{\left|(\nabla u)^x_{j,k}\right|^2 + \left|(\nabla u)^y_{j,k}\right|^2}, \end{aligned} \tag{9}$$

where $j = 1,\cdots,m, k = 1,\cdots,n$, $u_{j,k}$ is the (j,k)th pixel location of the image u. And $(\nabla u)^x_{j,k}$ and $(\nabla u)^y_{j,k}$ denote the horizontal and vertical first-order difference, respectively,

$$\begin{aligned}(\nabla u)^x_{j,k} &= \begin{cases} u_{j+1,k} - u_{j,k}, & \text{if } j < m, \\ 0, & \text{if } j = m, \end{cases} \\ (\nabla u)^y_{j,k} &= \begin{cases} u_{j,k+1} - u_{j,k}, & \text{if } k < n, \\ 0, & \text{if } k = n. \end{cases} \end{aligned} \tag{10}$$

B. ADDITIVE STRUCTURED NOISE REMOVE

Let us review the previous works in [23], [24] briefly about generating and solving structured noise. In [24], Fehrenbach et al. used a stationary noise assumption to replace the white noise assumption. Based on this new additive noise assumption, the additive degradation model can be rewritten as: $u_0 = u + \sum_{i=1}^{mn} \psi_i \star \nu_i$. The operator ψ_i is a known elementary pattern, to represent the image structural information. The vector ν_i follows white noise with known probability density functions. The model was proposed to restore images affected by additive structured noise as follows,

$$\min_{\nu_i} \left\| \nabla \left(u_0 - \sum_{i=1}^{mn} \psi_i \star \nu_i \right) \right\|_1 + \sum_{i=1}^{mn} \phi_i(\nu_i), \tag{11}$$

where the first term is TV regularization term; the second term is data fitting term which depends on the probability distribution of ν_i, and $\phi_i(\nu_i)$ is Tikhonov regularization [61]. They exploited primal-dual algorithms to solve this model, and obtained good numerical results for restoring image under additive structured noise.

C. MULTIPLICATIVE STRUCTURED NOISE REMOVE

In [23], Escande et al. proposed a convex model to restore images with multiplicative structured noise. Here, the degradation model can be rewritten as

$$u_0 = u \oslash \delta, \tag{12}$$

where $\delta = \psi \star \lambda$, and λ is noise that follows Gamma distribution. The point-wise division between two elements u and δ is denoted $(u \oslash \delta)[i] = u[i]/\delta[i]$. Based on this degradation model, a convex variation model to recover

TABLE 1. ReErr, MSSIM and PSNR for Gaussian blur.

				Observed				Restored		
Images	Blur	Noise	K	ReErr	MSSIM	PSNR	Models	ReErr	MSSIM	PSNR
peppers	GB(5,2)	stripes	1	0.1192	0.6991	23.22	AA	0.0942	0.7461	25.27
							HNZ	0.0902	0.7453	25.65
							DZ	0.0784	0.7617	26.87
							WZ	0.0876	0.7810	25.90
							LY	0.0807	0.7675	26.62
							OUR	**0.0767**	**0.7979**	**27.06**
	GB(7,2)			0.1217	0.6766	23.05	AA	0.0971	0.7243	25.01
							HNZ	0.1054	0.7155	24.29
							DZ	0.0850	0.7465	26.17
							WZ	0.0927	0.7244	25.41
							LY	0.0881	0.7405	25.85
							OUR	**0.0842**	**0.7559**	**26.24**
	GB(5,5)			0.1214	0.6830	23.07	AA	0.0969	0.7372	25.03
							HNZ	0.0920	0.7414	25.48
							DZ	0.0817	0.7541	26.51
							WZ	0.0884	0.7764	25.82
							LY	0.0833	0.7589	26.34
							OUR	**0.0810**	**0.7830**	**26.58**
f16	GB(5,2)	stripes	1	0.1242	0.6461	20.07	AA	0.1045	0.7263	21.56
							HNZ	0.0757	0.7691	24.36
							DZ	0.0752	0.7642	24.44
							WZ	0.0679	0.7952	25.31
							LY	0.0748	0.7811	24.47
							OUR	**0.0605**	**0.8459**	**26.31**
	GB(7,2)			0.1288	0.6131	19.75	AA	0.1104	0.6942	21.09
							HNZ	0.0868	0.7344	21.17
							DZ	0.0803	0.7474	23.86
							WZ	0.0737	0.7722	24.60
							LY	0.0821	0.7456	23.66
							OUR	**0.0702**	**0.7792**	**25.02**
	GB(5,5)			0.1269	0.6255	19.88	AA	0.1073	0.7094	21.34
							HNZ	0.0744	0.7626	24.17
							DZ	0.0772	0.7569	24.19
							WZ	0.0699	0.7872	25.05
							LY	0.0767	0.7681	24.25
							OUR	**0.0651**	**0.8261**	**25.68**
zedla	GB(5,2)	stripes	0.15	0.1996	0.5643	19.45	AA	0.1227	0.6876	23.68
							HNZ	0.0906	0.7443	26.31
							DZ	0.0873	0.7461	26.63
							WZ	0.1084	0.7281	24.76
							LY	0.0894	0.7339	26.43
							OUR	**0.0774**	**0.7740**	**27.68**
	GB(7,2)			0.1962	0.5453	19.60	AA	0.1221	0.6725	23.72
							HNZ	0.0988	0.7267	25.56
							DZ	0.0918	0.7306	26.20
							WZ	0.1073	0.7221	24.85
							LY	0.0953	0.6982	25.88
							OUR	**0.0817**	**0.7602**	**27.21**
	GB(5,5)			0.1998	0.5519	19.44	AA	0.1247	0.6801	25.41
							HNZ	0.0921	0.7396	26.17
							DZ	0.0892	0.7401	26.45
							WZ	0.1185	0.6997	25.99
							LY	0.0925	0.7251	26.13
							OUR	**0.0799**	**0.7604**	**27.40**

images affected by multiplicative structured noise is proposed as follows,

$$\min_{\lambda} c \left\| \nabla \left(u_0 \odot (\psi \star \lambda) \right) \right\|_1 + \langle b\lambda - (a-1)\log\lambda, 1 \rangle, \quad (13)$$

where c is the parameter to balance the TV term and the data fidelity term; the parameters (a and b) are from Gamma distribution. This model can handle the problem of images with multiplicative structured noise well. However, the blurring effect is unavoidable and not taken into account in [23]. Thereby, in this paper, we consider the deblurring issues under multiplicative structured noise.

III. THE PROPOSED MODEL

A. IMAGING PIPELINE

The classical blurred images with multiplicative noise degradation model is like (1)

$$u_0 = Hu \odot \eta.$$

TABLE 2. ReErr, MSSIM and PSNR for motion blur.

				Observed				Restored		
Images	Blur	Noise	K	ReErr	MSSIM	PSNR	Models	ReErr	MSSIM	PSNR
peppers	MB(3,0)	stripes	1	0.1144	0.7724	23.58	AA	0.0814	0.7975	26.54
							HNZ	0.0668	0.7949	28.25
							DZ	0.0650	0.7948	28.58
							WZ	0.0621	0.8325	28.88
							LY	0.0730	0.8248	27.47
							OUR	**0.0566**	**0.8367**	**29.66**
	MB(5,0)			0.1155	0.7423	23.50	AA	0.0850	0.7757	26.16
							HNZ	0.0905	0.7649	26.43
							DZ	0.0722	0.7784	27.58
							WZ	0.0761	0.7558	27.12
							LY	0.0655	0.8193	27.96
							OUR	**0.0667**	**0.8314**	**28.26**
	MB(5,30)			0.1167	0.7322	23.41	AA	0.0891	0.7594	25.75
							HNZ	0.0859	0.7557	26.07
							DZ	0.0733	0.7740	27.45
							WZ	0.0706	0.8197	27.77
							LY	0.0734	0.8021	27.44
							OUR	**0.0696**	**0.8201**	**27.90**
f16	MB(3,0)	stripes	1	0.1128	0.7353	20.90	AA	0.0885	0.8102	23.01
							HNZ	0.0553	0.8331	27.08
							DZ	0.0646	0.7977	25.74
							WZ	0.0588	0.8909	26.56
							LY	0.0594	0.8629	26.47
							OUR	**0.0402**	**0.9242**	**29.87**
	MB(5,0)			0.1191	0.6887	20.43	AA	0.0959	0.7722	22.31
							HNZ	0.0682	0.7973	25.28
							DZ	0.0697	0.7832	25.09
							WZ	0.0633	0.8599	25.92
							LY	0.0652	0.8321	25.66
							OUR	**0.0529**	**0.8837**	**27.48**
	MB(5,30)			0.1199	0.6802	20.37	AA	0.0982	0.7529	22.11
							HNZ	0.0709	0.7882	24.93
							DZ	0.0710	0.7796	24.92
							WZ	0.0732	0.8511	24.66
							LY	0.0691	0.8174	25.19
							OUR	**0.0548**	**0.8731**	**27.17**
zedla	MB(3,0)	stripes	0.15	0.2000	0.6099	19.44	AA	0.1232	0.7179	23.65
							HNZ	0.0856	0.7753	26.81
							DZ	0.0780	0.7737	27.62
							WZ	0.1450	0.6099	22.23
							LY	0.0933	0.7617	26.06
							OUR	**0.0646**	**0.8398**	**29.25**
	MB(5,0)			0.2074	0.5762	19.12	AA	0.1243	0.6978	24.74
							HNZ	0.0897	0.7521	26.40
							DZ	0.0835	0.7552	27.03
							WZ	0.1290	0.7336	23.27
							LY	0.0917	0.7526	26.21
							OUR	**0.0743**	**0.8038**	**28.04**
	MB(5,30)			0.2012	0.5829	19.39	AA	0.1207	0.6958	23.83
							HNZ	0.0886	0.7524	26.51
							DZ	0.0834	0.7531	27.03
							WZ	0.1226	0.7044	23.69
							LY	0.0878	0.7550	25.58
							OUR	**0.0725**	**0.8075**	**28.25**

Based on this degraded function, many approaches were proposed to deal with blurring issues. However, this equation leads to serious numerical troubles since the MAP estimator is non-convex, like the AA model. To avoid the numerical difficulties, similarly to [23], let u denote the original image and u_0 denote the observed image, λ is the multiplicative noise, and H is a blurred operator, we change the degradation model as follows,

$$u_0 = Hu \oslash \delta, \tag{14}$$

where $\delta = \psi \star \lambda$, the vector λ follows Gamma distribution, and its density function is

$$P(x; b, \alpha) = \frac{b^\alpha}{\tau(\alpha)} x^{\alpha-1} \exp(-bx), \tag{15}$$

where $\tau(\alpha)$ is the Gamma function. The parameter $a > 0$ is called the shape parameter, the parameter $b > 0$ is called the inverse scale parameter. The advantages of (14) are as follows:

TABLE 3. ReErr, MSSIM and PSNR for average blur.

				Observed				Restored		
Images	Blur	Noise	K	ReErr	MSSIM	PSNR	Models	ReErr	MSSIM	PSNR
peppers	AB(3)	stripes	1	0.1156	0.7407	23.50	AA	0.0898	0.7855	25.68
							HNZ	0.0739	0.7800	27.38
							DZ	0.0699	0.7818	27.87
							WZN	0.0792	0.8302	26.77
							LY	0.0683	0.8051	28.06
							OUR	**0.0652**	**0.8345**	**28.46**
	AB(5)			0.1219	0.6799	23.03	AA	0.0973	0.7356	24.99
							HNZ	0.0923	0.7405	25.45
							DZ	0.0822	0.7528	26.45
							WZN	0.0872	0.7622	26.35
							LY	0.0838	0.7572	26.29
							OUR	**0.0809**	**0.7791**	**26.60**
f16	AB(3)	stripes	1	0.1169	0.7004	20.59	AA	0.0954	0.7744	22.35
							HNZ	0.0609	0.8158	26.26
							DZ	0.0681	0.7866	25.29
							WZN	0.0549	0.8414	27.16
							LY	0.0667	0.8238	25.46
							OUR	**0.0483**	**0.8933**	**28.27**
	AB(5)			0.1274	0.6214	19.85	AA	0.1079	0.7058	21.29
							HNZ	0.0777	0.7613	24.14
							DZ	0.0777	0.7552	24.13
							WZN	0.0671	0.7941	25.40
							LY	0.0775	0.7653	24.17
							OUR	**0.0664**	**0.8190**	**25.50**
zelda	AB(3)	stripes	0.15	0.1972	0.5978	19.56	AA	0.1230	0.7090	23.66
							HNZ	0.0925	0.7385	26.13
							DZ	0.0800	0.7644	27.39
							WZN	0.1420	0.7415	22.41
							LY	0.0924	0.7430	26.14
							OUR	**0.0681**	**0.8255**	**28.80**
	AB(5)			0.1999	0.5494	19.44	AA	0.1251	0.6797	23.51
							HNZ	0.0864	0.7689	26.73
							DZ	0.0882	0.7373	26.55
							WZN	0.1204	0.6939	23.84
							LY	0.0936	0.7222	26.02
							OUR	**0.0840**	**0.7765**	**26.97**

TABLE 4. The CPU-time(s).

	Models	GB(5,2)	GB(7,2)	GB(5,5)	MB(3)	MB(5)	MB(5,30)	AB(3)	AB(5)
peppers	AA	26.31	28.60	26.63	23.55	26.87	27.44	22.72	26.13
	HNZ	21.55	22.11	22.63	19.34	19.95	21.58	21.20	22.58
	DZ	28.63	27.30	37.49	49.64	46.10	45.28	43.08	34.89
	WZN	7.46	8.16	7.75	35.69	39.36	36.00	8.60	10.60
	LY	13.46	12.89	13.68	13.70	13.79	13.90	14.35	13.32
	OUR	**3.94**	**3.88**	**3.72**	**3.40**	**3.73**	**3.99**	**4.35**	**3.76**
f16	AA	15.00	15.09	15.94	18.44	17.78	17.59	16.81	14.09
	HNZ	21.36	19.02	21.75	18.48	19.88	20.20	20.56	20.97
	DZ	28.07	25.33	28.43	36.04	33.19	20.74	35.20	26.64
	WZN	6.10	6.52	6.17	15.49	14.20	10.10	6.99	7.62
	LY	6.13	5.80	6.01	6.98	6.53	6.32	6.42	5.92
	OUR	**3.75**	**3.80**	**3.67**	**3.67**	**3.59**	**3.60**	**3.67**	**3.59**
zelda	AA	51.67	54.20	49.69	47.13	49.97	52.27	47.52	46.15
	HNZ	23.40	22.20	26.45	20.69	23.02	22.80	21.75	25.77
	DZ	95.95	92.04	99.50	81.62	82.49	83.19	86.39	76.38
	WZN	**4.28**	4.36	4.67	7.36	4.64	4.43	**4.64**	4.80
	LY	8.17	7.92	8.30	8.92	8.58	8.23	8.82	7.98
	OUR	4.29	**4.02**	**4.30**	**3.32**	**3.35**	**3.35**	4.86	**3.38**

- We rewrite multiplication into the division, it makes u and λ become a linear system to overcome numerical troubles because of using MAP estimator.
- In this degradation model, we consider the factors of the blurring, multiplicative noise, and structure. The model can more accurately reflect coherent imaging systems, such as SAR, Single Plane Illumination Microscope (SPIM), and Atomic Force Microscope (AFM) imaging.

B. THE PROPOSED MODEL VIA THE MAP ESTIMATOR

In this section, based on (14), we propose a convex model to restore blurred images with multiplicative structured noise.

TABLE 5. Restored results of images are degraded by different structured types.

				Observed				Restored			
Images	Blur	Noise	K	ReErr	MSSIM	PSNR	Models	ReErr	MSSIM	PSNR	CPU-time(s)
peppers	MB(5)	speckle	5	0.1789	0.7492	19.70	AA	0.1042	0.7603	21.82	29.61
							HNZ	0.0906	0.7286	25.61	32.28
							DZ	0.0912	0.7617	25.55	68.47
							WZN	0.1065	0.7760	24.21	15.38
							LY	0.1023	0.7656	24.55	14.92
							OUR	**0.0791**	**0.7939**	**26.79**	**5.73**
f16	MB(5)	grid	5	0.1178	0.7259	20.53	AA	0.0858	0.8233	23.27	20.53
							HNZ	0.0763	0.7524	24.30	32.61
							DZ	0.0730	0.8436	24.68	18.26
							WZN	0.0759	0.7769	24.34	13.48
							LY	0.0703	0.8154	24.75	6.37
							OUR	**0.0712**	**0.8587**	**24.90**	**3.94**
zelda	MB(5)	point	33	0.5406	0.3407	10.80	AA	0.4714	0.5423	11.99	91.56
							HNZ	0.1499	0.7470	21.94	21.80
							DZ	0.4272	0.4671	12.84	105.48
							WZN	0.3708	0.4880	14.07	80.25
							LY	0.3181	0.4355	15.40	8.06
							OUR	**0.1080**	**0.7547**	**24.79**	**4.05**

TABLE 6. Restored results of images degraded by different noise levels.

				Observed				Restored			
Images	Blur	Noise	K	ReErr	MSSIM	PSNR	Models	ReErr	MSSIM	PSNR	CPU-time(s)
peppers	GB(5,2)	stripes	0.1	0.2813	0.4631	15.77	AA	0.2186	0.5949	17.96	56.11
							HNZ	0.1855	0.6708	19.38	53.28
							DZ	0.1980	0.6614	18.82	105.48
							WZN	0.2102	0.6468	18.30	3.76
							LY	0.1766	0.6498	19.81	10.28
							OUR	**0.1716**	**0.7047**	**20.06**	**4.06**
			0.5	0.1492	0.6410	21.28	AA	0.1128	0.7184	23.71	29.94
							HNZ	0.0980	0.7453	24.71	37.99
							DZ	0.1105	0.7514	23.89	39.77
							WZN	0.1282	0.7396	22.60	76.49
							LY	0.0850	0.7515	26.16	14.26
							OUR	**0.0787**	**0.7920**	**26.83**	**3.97**
			1.5	0.1080	0.7273	24.08	AA	0.0866	0.7580	26.00	29.94
							HNZ	0.0913	0.7453	25.54	21.16
							DZ	0.0822	0.7654	26.46	36.17
							WZN	0.0737	0.8007	27.40	17.52
							LY	0.0799	0.7735	26.70	14.01
							OUR	**0.0734**	**0.8016**	**27.43**	**4.68**

We assume that $P(x)$ is the probability of variable x and $P(x|y)$ is the probability of x on observation y. Our target is to maximize $P(u, \lambda\,|u_0)$. Using Bayes rules, we have

$$P(u, \lambda\,|u_0\,) = \frac{P(u_0\,|u, \lambda\,)P(u, \lambda)}{P(u_0)}. \tag{16}$$

By taking the negative logarithmic transformation, this problem can be rewritten as follows,

$$-\log(P(u_0\,|u, \lambda\,)) - \log P(u, \lambda) + \log P(u_0). \tag{17}$$

Because u and λ are independent, we can get $P(u, \lambda) = P(u)P(\lambda)$. Moreover, the clean image u and the observed image u_0 satisfy the linear relation. It means that $P(u_0\,|u, \lambda)$ and $P(u_0)$ are constants [24]. In this paper, we assume that images have a low total variation, which can be expressed as

$$P(u) \propto \exp\left(-c\|\nabla u\|_1\right). \tag{18}$$

As λ follows Gamma distribution, we can get the data fitting term. By introducing the constraint condition: $u_0 = Hu \oslash (\psi \star \lambda)$, we can get the restoration model finally,

$$\begin{aligned} &\min_{u,\lambda} \langle b\lambda - (\alpha - 1)\log\lambda, 1\rangle + c\|\nabla u\|_1, \\ &\text{s.t. } Hu = u_0 \odot (\psi \star \lambda). \end{aligned} \tag{19}$$

The proposed model (19) is convex if we can keep the parameters $\alpha > 1, b > 0$. By introducing auxiliary variable y and z, model (19) can be rewritten as

$$\begin{aligned} &\min_{u,\lambda} \langle b\lambda - (\alpha - 1)\log\lambda, 1\rangle + c\|z\|_1, \\ &\text{s.t. } Hu = u_0 \odot (\psi \star y), \quad \nabla u = z,\ \lambda = y. \end{aligned} \tag{20}$$

IV. NUMERICAL METHOD

Let's start a general convex minimization model with separable structures,

$$\begin{aligned} &\min f(x_1) + g(x_2) + q(x_3), \\ &\text{s.t. } A_1x_1 + A_2x_2 + A_3x_3 = b, \\ &\quad x_i \in \mathcal{X}_i, \quad i = 1, 2, 3, \end{aligned}$$

TABLE 7. Restored results from different models and algorithms.

			Observed				Restored			
Image	Noise	K	ReErr	MSSIM	PSNR	Models	ReErr	MSSIM	PSNR	CPU-time(s)
f16	stripes	1	0.1093	0.7765	21.17	AA	0.0777	0.8529	24.14	24.14
						DZ	0.0680	0.8887	25.30	1.98
						EWZ	0.0441	0.9502	29.05	14.66
						WZN	0.0786	0.8526	24.04	5.09
						LY	0.0787	0.8382	24.03	6.74
						OUR	**0.0323**	**0.9664**	**31.77**	**3.58**

where $f(x_1)$, $g(x_2)$, and $q(x_3)$ are lower semicontinuous proper convex function; A_i are given matrices; b is a known vector; $\mathcal{X}_i$ are nonempty closed convex sets. Hence, the convex optimization model (20) falls into the above form with the following specifications:

- $x_1 := u$, $x_2 := \lambda$, $x_3 := (y, z)$, and the abstract sets are $\mathcal{X}_i := \mathbb{R}^n$;
- $f(x_1) = 0$, $g(x_2) = b\lambda - (\alpha - 1)\log\lambda$, and $q(x_3) = c\|z\|_1$;
- the matrices A_i and b are given by, respectively:

$$A_1 := \begin{pmatrix} H/(u_0 \odot \psi) \\ \nabla \\ 0 \end{pmatrix}, \quad A_2 := \begin{pmatrix} 0 \\ 0 \\ I \end{pmatrix},$$
$$A_3 := \begin{pmatrix} -I & 0 \\ 0 & -I \\ -I & 0 \end{pmatrix}, \quad b = \begin{pmatrix} 0 \\ 0 \\ 0 \end{pmatrix},$$

where I is the identity operator. The augmented Lagrangian function of the model (20) is given by

$$\begin{aligned} &\mathcal{L}(z, u, \lambda, y; \omega_1, \omega_2, \omega_3) \\ &= c\|z\|_1 + \langle \omega_1, \nabla u - z\rangle + \frac{\mu_1}{2}\|\nabla u - z\|_2^2 \\ &\quad + \langle \omega_2, Hu - u_0 \odot (\psi \star y)\rangle + \frac{\mu_2}{2}\|Hu - u_0 \odot (\psi \star y)\|_2^2 \\ &\quad + \langle \omega_3, \lambda - y\rangle + \frac{\mu_3}{2}\|\lambda - y\|_2^2 + \langle b\lambda - (\alpha - 1)\log\lambda, 1\rangle, \end{aligned} \tag{21}$$

where ω_1, ω_2, and ω_3 are the Lagrangian multipliers, μ_1, μ_2, and μ_3 are the penalty parameters. The augmented Lagrangian method (ALM) for problem (21) is an iterative algorithm based on the iteration,

$$\begin{cases} \left(z^{k+1}, u^{k+1}, \lambda^{k+1}, y^{k+1}\right) \\ \qquad = \arg\min_{z,u,\lambda,y} \mathcal{L}\left(z, u, \lambda, y; \omega_1^k, \omega_2^k, \omega_3^k\right), & \text{(22a)} \\ \omega_1^{k+1} = \omega_1^k + \theta\mu_1\left(\nabla u^{k+1} - z^{k+1}\right), & \text{(22b)} \\ \omega_2^{k+1} = \omega_2^k + \theta\mu_2\left(Hu^{k+1} - u_0 \odot (\psi \star y^{k+1})\right), & \text{(22c)} \\ \omega_3^{k+1} = \omega_3^k + \theta\mu_3(\lambda^{k+1} - y^{k+1}). & \text{(22d)} \end{cases}$$

We apply the alternating direction method of multipliers (ADMM) to the minimization of $\mathcal{L}(z, u, y, \lambda; \omega_1, \omega_2, \omega_3)$ in (21),

$$\begin{cases} z^{k+1} = \arg\min_z c\|z\|_1 - \left\langle \omega_1^k, z\right\rangle \\ \qquad + \frac{\mu_1}{2}\left\|\nabla u^k - z\right\|_2^2, & \text{(23a)} \\ u^{k+1} = \arg\min_u \left\langle \omega_1^k, \nabla u\right\rangle + \frac{\mu_1}{2}\left\|\nabla u - z^{k+1}\right\|_2^2 \\ \qquad + \left\langle \omega_2^k, Hu\right\rangle + \frac{\mu_2}{2}\left\|Hu - u_0 \odot (\psi \star y^k)\right\|_2^2, & \text{(23b)} \\ \lambda^{k+1} = \arg\min_\lambda \langle b\lambda - (\alpha - 1)\log\lambda, 1\rangle \\ \qquad + \left\langle \omega_3^k, \lambda\right\rangle + \frac{\mu_3}{2}\left\|\lambda - y^k\right\|_2^2, & \text{(23c)} \\ y^{k+1} = \arg\min_y -\left\langle \omega_2^k, u_0 \odot (\psi \star y)\right\rangle \\ \qquad + \frac{\mu_2}{2}\left\|Hu^{k+1} - u_0 \odot (\psi \star y)\right\|_2^2 \\ \qquad - \left\langle \omega_3^k, y\right\rangle + \frac{\mu_3}{2}\left\|\lambda^{k+1} - y\right\|_2^2. & \text{(23d)} \end{cases}$$

A. Z SUBPROBLEM

For z subproblem, we can use the shrinkage operator to solve directly,

$$z^{k+1} = \text{shrink}\left(\nabla u^k + \frac{\omega_1}{\mu_1}, \frac{c}{\mu_1}\right), \tag{24}$$

where the shrinkage operator shrink $\left(\cdot, \frac{c}{\mu_1}\right)$ is defined by

$$\text{shrink}\left(\xi, \frac{c}{\mu_1}\right) \triangleq \max\left\{|\xi| - \frac{c}{\mu_1}, 0\right\} \cdot \frac{\xi}{|\xi|}. \tag{25}$$

Especially, the element $\frac{\xi}{|\xi|}$ should be taken as 0 if $|\xi| = 0$.

B. U SUBPROBLEM

For fixed z, y, λ, the minimization of $\mathcal{L}$ with respect to u can be rewritten as follows,

$$M_u u^{k+1} = r_u^k, \tag{26}$$

where

$$\begin{aligned} M_u &= \mu_1\nabla^T\nabla + \mu_2 H^T H, \\ r_u^k &= \mu_1\nabla^T z^{k+1} + \mu_2 H^T(u_0 \odot (\psi \star y^k)) - H^T\omega_2^k - \nabla^T\omega_1^k. \end{aligned} \tag{27}$$

Under the periodic boundary condition for u, we know that $\nabla^T\nabla$ and $H^T H$ are block circulation, so we can use the fast

(a) peppers (b) f16 (c) zelda (d) band

FIGURE 1. The original images. (a), (b) and (c) are synthetic images, (d) is a real image.

(a) no structured noise (b) speckle (c) stripes (d) grid (e) line (f) flow

FIGURE 2. Common types of structured noise.

Fourier transform (FFT) to find the solution of this subproblem efficiently,

$$\mathcal{F}^\top \hat{M}_u \mathcal{F} u^{k+1} = r_u^k, \tag{28}$$

$$u^{k+1} = \mathcal{F}^\top \hat{M}_u^{-1} \mathcal{F} r_u^k, \tag{29}$$

where $\hat{M}_u = \mathcal{F}(\mu_1 \nabla^T \nabla + \mu_2 H^T H)\mathcal{F}^\top$.

C. λ SUBPROBLEM

For this subproblem, this problem can be rewritten as

$$b - \frac{\alpha - 1}{\lambda} + \omega_3^k + \mu_3(\lambda - y^k) = 0, \tag{30}$$

then this question can be solved by

$$\lambda = \frac{-Tep + \sqrt{Tep^2 + 4(\alpha - 1)\mu_3}}{2\mu_3}, \tag{31}$$

where $Tep = b + \omega_3^k - \mu_3 y^k$.

D. Y SUBPROBLEM

For y subproblem, this problem is equal to

$$(\mu_2 u_0^2 \psi^T \psi + \mu_3 I) y = u_0 \psi^T \omega_2^k + H\mu_2 u_0 \psi^T u^{k+1} + \omega_3^k I + \lambda^{k+1}\mu_3. \tag{32}$$

We use Preconditioned Conjugate Gradients Method (termed "PCG") to solve (32). This method is based on the conjugate gradient method, which can improve the speed of the algorithm by preprocessing. Assuming that the preconditioned matrix P is symmetric and positive definite, the linear equations $AY = B$ can be transformed into

$$Q^{-1}AY = Q^{-1}B. \tag{33}$$

If $Q^{-1}A$ has smaller condition number than A, it can improve the speed of solving this system of linear equations. Using this method, the condition is that A is symmetric and positive definite, and B is known. In this subproblem, we have

$$A = \mu_2 u_0^2 \psi^T \psi + \mu_3 I,$$
$$B = u_0 \psi^T \omega_2^k + H\mu_2 u_0 \psi^T u^{k+1} + \omega_3^k I + \lambda^{k+1}\mu_3.$$

Because $\psi^T \psi$ as symmetric and positive definite, $\mu_3 I$ is a diagonal matrix, we know that A is symmetric and positive definite, and B is known. It means that the y subproblem can be solved by this method. We use MATLAB built-in "PCG" function to solve,

- X = PCG(A, B, TOL, MAXIT).

We set TOL as $1e^{-5}$; MAXIT is the maximum number of iterations (i.e., we set MAXIT is 40). The overall algorithm is summarized in Algorithm 1.

V. NUMERICAL EXPERIMENTS

In this section, we use four images which are given in Figure 1 as our testing images to display the effectiveness of the proposed method, labeled by "peppers" (512 × 512), "f16" (512 × 512), "zelda" (512 × 512), and "band" (512 × 512). Besides, "peppers", "f16", and "zelda" are synthetic images, and "band" is a real image. All the experiments are performed under Windows 10 and MATLAB R2019b running on a Notebook PC with an Intel

FIGURE 3. The top row: showing three clean images. The second row: showing images only affected by structured noise (stripes noise). The third row: showing images only affected by average blur (AB (10)). Bottom row: showing the images are affected by average blur and stripes noise.

Core (TM) i7-8565U CPU at 1.80 GHz with 8 GB of RAM. Quantitatively, the quality of the recovered images is evaluated by the peak signal-to-noise ratio (PSNR), the relative error (ReErr), and structural similarity (SSIM) [62]. The PSNR and ReErr are defined as,

$$\mathrm{PSNR} = 10\log\frac{mn\max(\max(u_0),\max(u))^2}{\|u_0-u\|^2}, \tag{34}$$

$$\mathrm{ReErr} = \frac{\|u_0-u\|^2}{\|u\|^2}, \tag{35}$$

where u_0 and u are the restored image and the original image, respectively. The size of these images is $m\times n$. And the SSIM [62] can be defined as follows,

$$\mathrm{SSIM}(x,y) = \frac{\left(2\mu_x\mu_y+\theta_1\right)\left(2\sigma_{xy}+\theta_2\right)}{\left(\mu_x^2+\mu_y^2+\theta_1\right)\left(\sigma_x^2+\sigma_y^2+\theta_2\right)}, \tag{36}$$

where μ_x, μ_y are the averages of x, y; σ_x^2, σ_y^2 are the variances; σ_{xy} is the covariance of x, y, and θ_1, θ_2 are two variables to stabilize the division with a weak denominator. The overall SSIM (MSSIM [63]) is the mean of local similarity indexes defined by

$$\mathrm{MSSIM} = \frac{1}{N}\sum_{i=1}^{N}\mathrm{SSIM}\left((x_i,y_i)\right), \tag{37}$$

where x_i, y_i are corresponding windows of clean/restored image indexed by i and N. Note that the larger PSNR,

(a) Degraded: 23.22. (b) AA model: 25.27. (c) HNZ model: 25.65. (d) DZ model: 26.87.

(e) WZN model: 25.90. (f) LY model: 26.62. (g) Our model: 27.06.

FIGURE 4. The recovering results of GB(5,2)/stripes/K = 1 for "peppers" with zoomed regions and PSNR values (db).

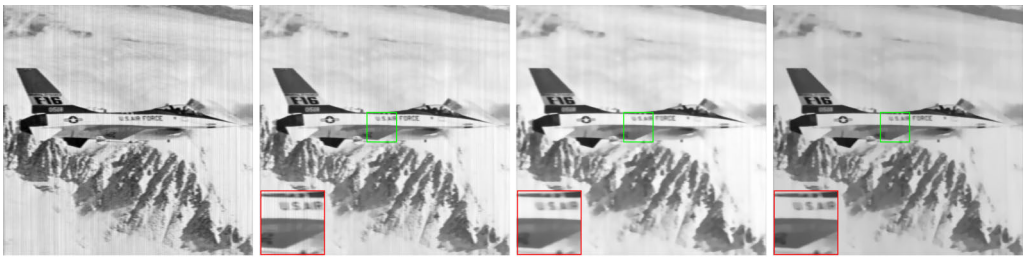

(a) Degraded: 23.81. (b) AA model: 27.43. (c) HNZ model: 26.26. (d) DZ model: 26.79.

(e) WZN model: 26.41. (f) LY model: 26.72. (g) Our model: 27.70.

FIGURE 5. The recovering results of MB(5)/stripes/K = 3 for "f16" with zoomed regions and PSNR values (db).

larger SSIM, and smaller ReErr means the better restoration effect. To illustrate the effectiveness of the proposed method, we compare the recovering results of our approach with those of the following image deblurring algorithms,

- **AA model** is proposed by Aubert and Aujol [26], and solved by the gradient method;
- **HNZ model** is proposed by Huang *et al.* [16], and solved by an alternating minimization algorithm;
- **DZ model** is proposed by Dong and Zeng [40], and solved by primal-dual algorithm;
- **WZN model** is proposed by Wang *et al.* [36], and solved by the ADMM algorithm;
- **LY model** is proposed by Lu *et al.* [50], and solved by an alternating minimization algorithm.

The HNZ model and DZ model are extensions of the AA model. The WZN model is a framelet-based convex optimization model for multiplicative noise and blur removal problems. Wang, Zhao, and Ng proposed a new method to select the regularization parameter by using the l_1 norm-based L-curve method for these framelet-based models. The LY model is a variational model and this model utilizes the

(a) Degraded: 24.90. (b) AA model: 27.44. (c) HNZ model: 25.24. (d) DZ model: 27.71.

(e) WZN model: 27.92. (f) LY model: 26.63. (g) Our model: 28.17.

FIGURE 6. The recovering results of AB(5)/stripes/K = 0.5 for "zelda" with zoomed regions and PSNR values (db).

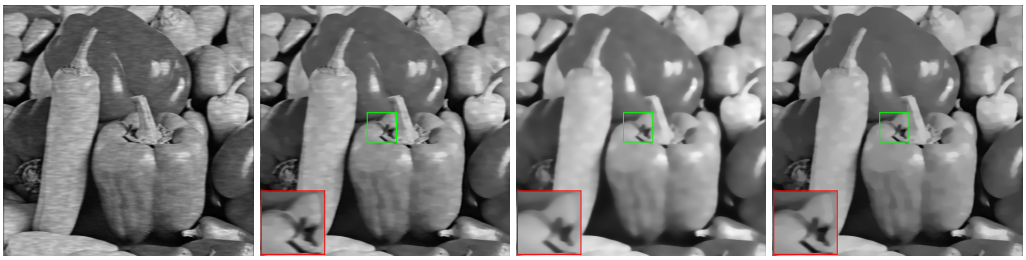

(a) Degraded: 19.70. (b) AA model: 21.82. (c) HNZ model: 25.61. (d) DZ model: 25.55.

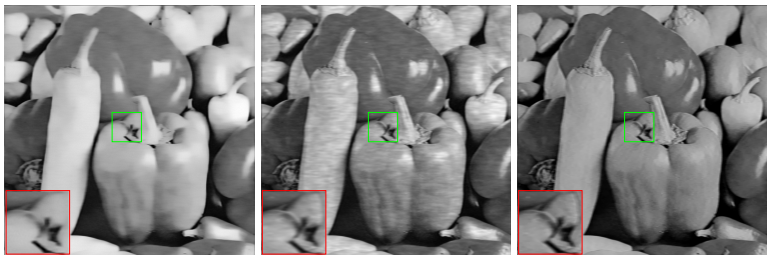

(e) WZN model: 24.21. (f) LY model: 24.55. (g) Our model: 26.79.

FIGURE 7. The recovering results of MB(5)/speckle/K = 5 for "peppers" with zoomed regions and PSNR values (db).

favorable properties of framelet regularization. These models can be used to solve the blurred images with multiplicative noise, and make competitive results for restoring blurred images with multiplicative Gamma noise. Without loss of generality, like the DZ model, we also assume that the mean of λ equals 1 under the multiplicative noise scheme. Let $K = \alpha$, $1/\theta = b$, then we have that $K\theta = 1$ and its variance is $1/K$. The density function (15) can be rewritten as

$$P(\lambda; \theta, K) = \frac{1}{\theta^K \tau(K)} \lambda^{K-1} e^{-\frac{\lambda}{\theta}}, \quad K > 1. \tag{38}$$

In our degradation model, we mainly consider three factors: Gamma noise levels, blur kernels, and structured noise types. Firstly, we use the MATLAB built-in function to generate the Gamma noise,

- random ("gamrnd", K, 1/K),

where the level of the Gamma noise is determined by the parameter K. Note that the smaller K is, the more serious the Gamma noise is. In all experiments, we choose different K numbers from the set of $K \in \{0.05, 0.15, 0.5, 1.5, 3, 5, 33\}$. For blur kernels, we consider three blur kernels ("Gaussian

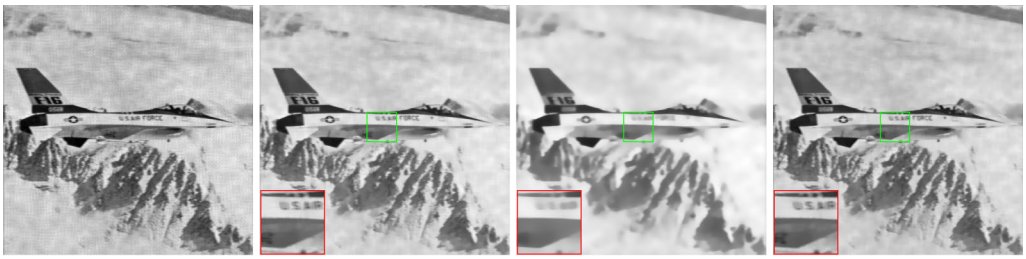

(a) Degraded: 20.53. (b) AA model: 23.27. (c) HNZ model: 24.30. (d) DZ model: 24.68.

(e) WZN model: 24.34. (f) LY model: 24.75. (g) Our model: 24.90.

FIGURE 8. The recovering results of MB(5)/grid/K = 5 for "f16" with zoomed regions and PSNR values (db).

(a) Degraded:10.80 (b) AA model: 11.99. (c) HNZ model: 21.94. (d) DZ model: 12.84.

(e) WZN model: 14.07. (f) LY model: 15.40. (g) Our model: 24.79.

FIGURE 9. The recovering results of MB(5)/point/K = 33 for "zelda" with zoomed regions and PSNR values (db).

blur", " motion blur", and "average blur"), and achieved by MATLAB command,

- "Gaussian blur" (GB): fspecial ("gaussian", pixels, sigma);
- "motion blur" (MB): fspecial ("motion", len, theta);
- "average blur" (AB): fspecial ("average", hsize).

For GB, we test three different sizes ($5 \times 2, 5 \times 5, 7 \times 2$); as for MB, we test three experiments. We test len = 3, 5 when the theta is the default number (i.e. theta = 0); when the theta = 30, the len is 5; about AB, we test hsize = 3, 5. Sure, in addition to these three common blur kernels, there are other blur kernels, such as "disk blur", "laplacian blur", "Sobel blur" and so on.

For structured noise types, we choose four types from six common structured noise types (see Figure 2), point, speckle, stripes, and grid noise, respectively. Speckle, stripes, and grid noise are common structured noise, point noise is multiplicative Gamma noise with no structure. As shown in Figure 3, the first row is the original images; the second row is the images only affected by multiplicative structured noise; the third row is the images only affected by blurring; the last row is the

(a) Degraded: 15.77. (b) AA model: 17.96. (c) HNZ model: 19.38. (d) DZ model: 18.82.

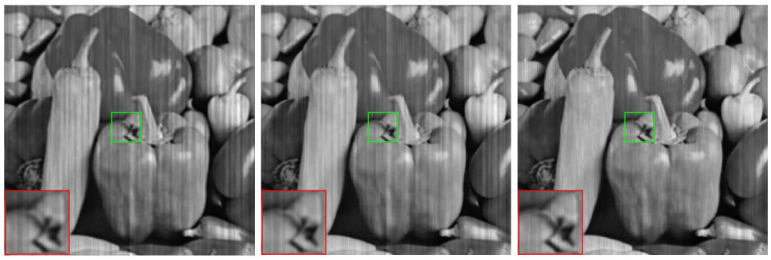

(e) WZN model: 18.30. (f) LY model: 19.81. (g) Our model: 20.06.

FIGURE 10. The recovering results of GB(5,2)/stripes/K = 0.1 for "peppers" with zoomed regions and PSNR values (db).

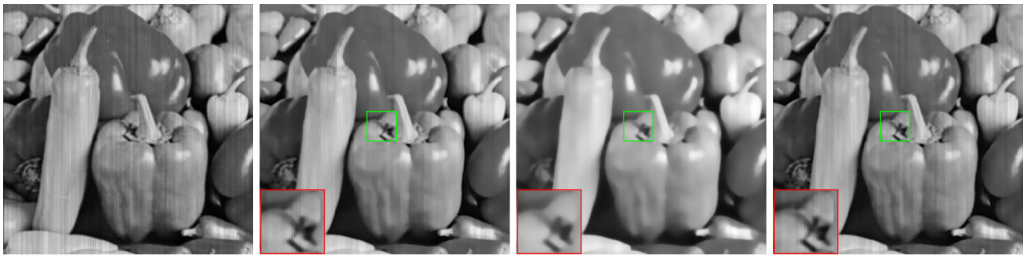

(a) Degraded: 21.28. (b) AA model: 23.71. (c) HNZ model: 24.71. (d) DZ model: 23.89.

(e) WZN model: 22.60. (f) LY model: 26.16. (g) Our model: 26.83.

FIGURE 11. The recovering results of GB(5,2)/stripes/K = 0.5 for "peppers" with zoomed regions and PSNR values (db).

images degraded by blurring and multiplicative structured noise.

A. PARAMETER SETTINGS

In our model, there are two parameters to control. To keep the convexity of the proposed model, we let $b > 0$, and $\alpha > 1$. We choose b from the set of $\{0.1, 0.3, 0.5, 1\}$. And about α, we choose the best one from $\{2, 3, 4, 5\}$. From all the structured noise, if the type we choose is speckle, flow or line noise, $(\alpha, b) = (5, 1)$; if the type we choose is stripes or grid noise, $(\alpha, b) = (2, 1)$; if the type we choose is point noise (no structure), $(\alpha, b) = (5, 0.1)$. In this paper, we use the ADMM algorithm to solve our model. About the regularization parameter c and the ADMM penalty parameters μ_1, μ_2, μ_3, we choose the best one from the set of {1, 2, 3, 4, 5, 6, 7, 8, 9, 10, 20, 50}. And it is based on different types of noise. After testing, we found that when $c = 2$, $\mu_1 = \mu_2 = \mu_3 = 8$, our algorithm has a good recovery effect on the selected test set. In all the experiments, the stop criterion is either $\frac{E(u^{k+1})-E(u^k)}{E(u^{k+1})} < 1e^{-4}$ or the maximum iterative number exceeds 500.

For the other methods (the AA, HNZ, DZ, WZN, and LY model), we choose the corresponding parameters such that the MSSIM result is highest.

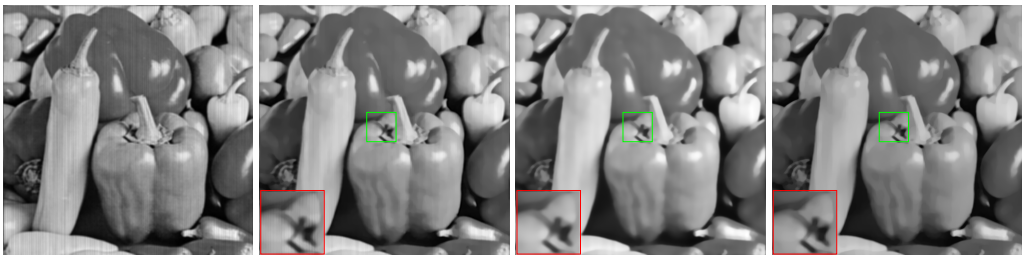

(a) Degraded: 24.08. (b) AA model: 26.00. (c) HNZ model: 25.54. (d) DZ model: 26.46.

(e) WZN model: 27.40. (f) LY model: 26.70. (g) Our model: 27.43.

FIGURE 12. The recovering results of GB(5,2)/stripes/K = 1.5 for "peppers" with zoomed regions and PSNR values (db).

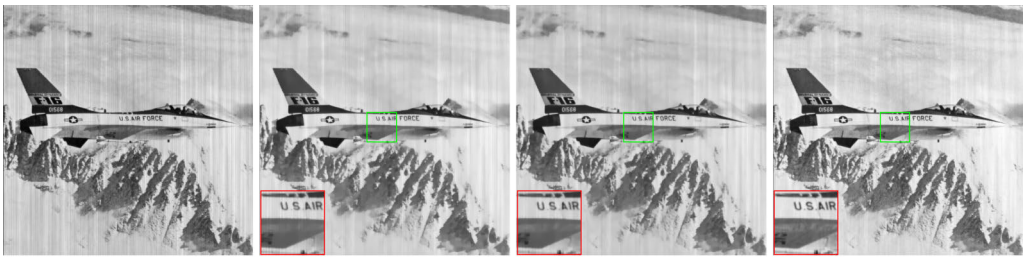

(a) Degraded: 21.27. (b) AA model: 24.14. (c) DZ model: 25.30. (d) EWZ model: 29.05.

(e) WZN model: 24.04. (f) LY model:24.03. (g) Our model: 31.77.

FIGURE 13. Restoration results of stripes/K = 1 for "f16" with zoomed regions and PSNR values (db).

B. EXPERIMENT 1

In the first experiment, the original images (including "peppers", "f16", and "zelda") are blurred by three different blur kernels, and further degraded by multiplicative structured noise. We choose stripes noise as structured noise in this experiment. And the K value (Gamma noise level) we set is 1 or 0.15. Tables 1-3 display the value of ReErr, MSSIM, and PSNR for three blurring kernels with different parameters. Table 4 lists the CPU-time of these six models. In Figure 4, we show the restored results of the Gaussian blur (GB(5,2)/K = 1). Figure 5 shows the partial restored effect of motion blur (MB(5)/K = 3). And we display the restoration results for average blur (AB(5)/K = 0.5) in Figure 6. All these results demonstrate our model can remove different blur kernels with structured noise effectively and also confirm that our proposed model gets better results than the other five models.

C. EXPERIMENT 2

In this experiment, we show the recovering results of the images degraded by different types of structured noise. The original image is corrupted by three different noise types

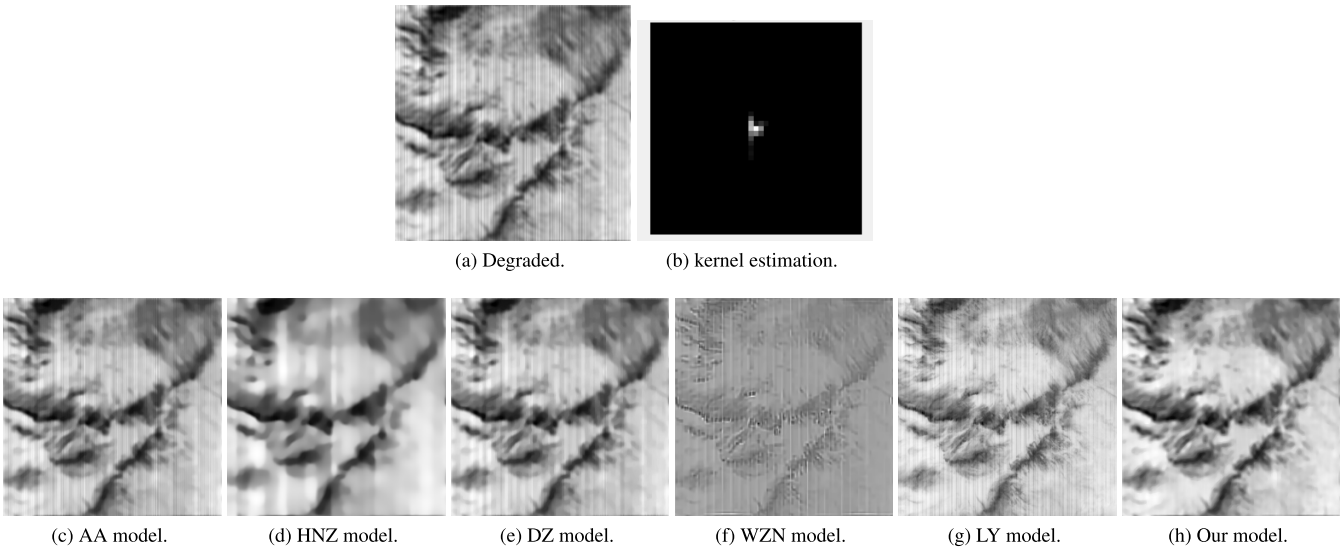

(a) Degraded. (b) kernel estimation.

(c) AA model. (d) HNZ model. (e) DZ model. (f) WZN model. (g) LY model. (h) Our model.

FIGURE 14. **The restored results of real image.**

Algorithm 1 ADMM for the Proposed Model

Input: the observed image u_0, psi, and the blur operation H.

Parameters: $\omega_1, \omega_2, \omega_3, \mu_1, \mu_2, \mu_3$, and stopping parameters tol.

Initialize: $u = u_0$, $\mu_1 = \mu_2 = \mu_3 = 0$, and $k = 0, 1, \ldots, Maxit$:

1. Compute z^{k+1} by (24),
2. Compute u^{k+1} by (29),
3. Compute λ^{k+1} by (31),
4. Compute y^{k+1} by (33),
5. Update ω_1^{k+1} by (22b),
6. Update ω_2^{k+1} by (22c),
7. Update ω_3^{k+1} by (22d).

If $\left\|u^{(k+1)} - u^{(k)}\right\| / \left\|u^{(k+1)}\right\| \leq tol$, stop.

Output: u^k.

including speckle noise, grid noise, and point noise (point noise without structure), and then this image is also blurred by MB (5). The degraded images and the recovered images are shown in Figures 7-9, respectively. The values of ReErr, MSSIM, and PSNR are shown in Table 5. These recovering results demonstrate that the proposed model is very effective to recover blurred images with different types of structured noise.

D. EXPERIMENT 3

In this experiment, we consider showing our model to restore images with different Gamma noise levels. We let ''peppers'' as our test image. Except for the noise levels, the image ''peppers'' is also corrupted by GB (5, 2) and stripes noise in this experiment. For Gamma noise, the smaller the K value is, the image degradation effect is more serious. We choose three different K numbers ($K = 0.1, 0.5, 1.5$). Table 6 tells that the proposed model improves the quality of restoration in terms of ReErr, MSSIM, and PSNR compared with the other models, and the speed is also better than the WZN, LY, DZ, AA, and HNZ models. Figures 10-12 show the degraded images with different K values and the corresponding recovered images, respectively.

E. EXPERIMENT 4

In Experiment 4, we consider a simplified model. When $H = Id$, it means that our model can be used to recover images that are only affected by multiplicative structured noise. Then, the ADMM algorithm in this paper can be compared with the primal-dual algorithm proposed by literature [23] (called the ''EWZ'' model), and the AA, DZ, WZN, and LY model. We choose the stripes noise as the structured noise, the K value is 1. The results are as follows. From Figure 13 and Table 7, although the DZ model takes the shortest time, our restoration effect is better significantly. In general, our model and algorithm are better than others.

F. EXPERIMENT 5

In the aforementioned four experiments, we mainly show the restoring effect on synthetic images. In this experiment, we show our model to recover the real image. Due to the complexity of the real image and the numerous influencing factors, we can only conduct qualitative analysis and compare them through visual effects. For the real image, it is important to estimate the blur kernel, and then use the no-blind method to estimate latent image. In this paper, we mainly propose a non-blind approach to restore the blurred image with multiplicative structured noise. In this experiment, we use the general Gaussian kernel to approach this real image blur kernel. There are two reasons to do this estimation. First, the Gaussian blur is widely used in the estimation of static

blur in natural imaging [64]–[66]; the second reason is that we use a blurring kernel estimation method proposed by [45] to estimate roughly. The kernel is shown as Figure 14(b), which is very much like the Gaussian blur height. The more accurate blur kernel estimation will be studied in our future work. Based on this kernel estimation, the restoration result is shown in Figure 14. It can be found that the recovery effect of our model is better.

VI. CONCLUSION

In this paper, we discuss the image restoration problems degraded by blurring and multiplicative structured noise, simultaneously. The most relevant conclusions are summarized as follows,

- A convex model based on the total variation (TV), the statistical property of the Gamma noise and the maximum a posteriori (MAP) estimator was proposed to restore degraded images with blurring and multiplicative structured noise, simultaneously.
- We employed an effective ADMM algorithm to handle this minimization problem, which is based on FFT, soft thresholding formula, and ''PCG'' method.
- We conduct many experiments on different blurring kernels, different types of structured noise, and different Gamma noise levels, and illustrate that the proposed model is robust and outperforms the state-of-the-art in image deblurring with multiplicative structured noise removing.
- Meanwhile, numerical results indicate that our algorithm can generate competitive results in terms of the CPU-time comparing to other algorithms and models.

REFERENCES

[1] C. Zhang, F. Zhou, B. Xue, and W. Xue, ''Stabilization of atmospheric turbulence-distorted video containing moving objects using the monogenic signal,'' *Signal Process., Image Commun.*, vol. 63, pp. 19–29, Apr. 2018.
[2] J. Wu, M. Dong, K. Ota, J. Li, and Z. Guan, ''FCSS: Fog-computing-based content-aware filtering for security services in information-centric social networks,'' *IEEE Trans. Emerging Topics Computing*, vol. 7, no. 4, pp. 553–564, Oct. 2019.
[3] Z. Yang, Z. Yang, and G. Gui, ''A convex constraint variational method for restoring blurred images in the presence of alpha-stable noises,'' *Sensors*, vol. 18, no. 4, p. 1175, Apr. 2018.
[4] K. Bredies, K. Kunisch, and T. Pock, ''Total generalized variation,'' *SIAM J. Imag. Sci.*, vol. 3, no. 3, pp. 492–526, 2010.
[5] J.-F. Cai, S. Osher, and Z. Shen, ''Split Bregman methods and frame based image restoration,'' *Multiscale Model. Simul.*, vol. 8, no. 2, pp. 337–369, Jan. 2010.
[6] A. Chambolle and P.-L. Lions, ''Image recovery via total variation minimization and related problems,'' *Numerische Math.*, vol. 76, no. 2, pp. 167–188, Apr. 1997.
[7] T. F. Chan and J. Shen, ''Theory and computation of variational image deblurring,'' in *Mathematics And Computation In Imaging Science And Information Processing*. Singapore: World Scientific, 2007, pp. 93–130.
[8] J. Pan, X. Yang, H. Cai, and B. Mu, ''Image noise smoothing using a modified Kalman filter,'' *Neurocomputing*, vol. 173, pp. 1625–1629, Jan. 2016.
[9] Z. Z. Yang and Z. Yang, ''Fast linearized alternating direction method of multipliers for the augmented ℓ_1-regularized problem,'' *Signal Image Video Process.*, vol. 9, no. 7, pp. 1601–1612, 2015.
[10] J.-H. Yang, X.-L. Zhao, T.-Y. Ji, T.-H. Ma, and T.-Z. Huang, ''Low-rank tensor train for tensor robust principal component analysis,'' *Appl. Math. Comput.*, vol. 367, Feb. 2020, Art. no. 124783.
[11] M. Lysaker and X.-C. Tai, ''Iterative image restoration combining total variation minimization and a second-order functional,'' *Int. J. Comput. Vis.*, vol. 66, no. 1, pp. 5–18, Jan. 2006.
[12] Z.-F. Pang, Y.-M. Zhou, T. Wu, and D.-J. Li, ''Image denoising via a new anisotropic total-variation-based model,'' *Signal Process., Image Commun.*, vol. 74, pp. 140–152, May 2019.
[13] Z.-G. Jia and M. Wei, ''A new TV-Stokes model for image deblurring and denoising with fast algorithms,'' *J. Sci. Comput.*, vol. 72, no. 2, pp. 522–541, Feb. 2017.
[14] B. Dong and Z. Shen, ''MRA based wavelet frames and applications,'' in *IAS Lecture Notes Series, Summer Program on the Mathematics of Image Processing*, vol. 19. Salt Lake City, UT, USA: Park City Mathematics Inst., 2010.
[15] J.-F. Cai, B. Dong, and Z. Shen, ''Image restoration: A wavelet frame based model for piecewise smooth functions and beyond,'' *Appl. Comput. Harmon. Anal.*, vol. 41, no. 1, pp. 94–138, Jul. 2016.
[16] Y. Huang, M. Ng, and T. Zeng, ''The convex relaxation method on deconvolution model withMultiplicative noise,'' *Commun. Comput. Phys.*, vol. 13, no. 4, pp. 1066–1092, Jun. 2015.
[17] A. Choux, L. Barnouin, L. Reverdy, and M. Theobald, ''Characterization of laser megajoule targets by X-ray tomography,'' *Fusion Sci. Technol.*, vol. 73, no. 2, pp. 127–131, Jan. 2018.
[18] Y. Shi, N. T. Lonnroth, R. E. Youngman, S. J. Rzoska, M. Bockowski, and M. M. Smedskjaer, ''Pressure-induced structural changes in titanophosphate glasses studied by neutron and X-ray total scattering analyses,'' *J. Non-Crystalline Solids*, vol. 483, pp. 50–59, Mar. 2018.
[19] R. I. Elsharif, B. A. Ibraheem, Z. A. Mustafa, S. K. Abass, and M. M. Fadl Allah, ''Wavelet Decomposition–Based speckle reduction method for ultrasound images by using speckle-reducing anisotropic diffusion and hybrid median,'' *J. Clin. Eng.*, vol. 43, no. 4, pp. 163–170, 2018.
[20] K. Singh, S. K. Ranade, and C. Singh, ''A hybrid algorithm for speckle noise reduction of ultrasound images,'' *Comput. Methods Programs Biomed.*, vol. 148, pp. 55–69, Sep. 2017.
[21] J. Yang, J. Fan, D. Ai, X. Wang, Y. Zheng, S. Tang, and Y. Wang, ''Local statistics and non-local mean filter for speckle noise reduction in medical ultrasound image,'' *Neurocomputing*, vol. 195, pp. 88–95, Jun. 2016.
[22] A. Pizurica, W. Philips, I. Lemahieu, and M. Acheroy, ''A versatile wavelet domain noise filtration technique for medical imaging,'' *IEEE Trans. Med. Imag.*, vol. 22, no. 3, pp. 323–331, Mar. 2003.
[23] P. Escande, P. Weiss, and W. Zhang, ''A variational model for multiplicative structured noise removal,'' *J. Math. Imag. Vis.*, vol. 57, no. 1, pp. 43–55, 2017.
[24] J. Fehrenbach, P. Weiss, and C. Lorenzo, ''Variational algorithms to remove stationary noise: Applications to microscopy imaging,'' *IEEE Trans. Image Process.*, vol. 21, no. 10, pp. 4420–4430, Oct. 2012.
[25] L. Rudin, P.-L. Lions, and S. Osher, ''Multiplicative denoising and deblurring: Theory and algorithms,'' in *Geometric Level Set Methods in Imaging, Vision, and Graphics*. New York, NY, USA: Springer, 2003, pp. 103–119.
[26] G. Aubert and J.-F. Aujol, ''A variational approach to removing multiplicative noise,'' *SIAM J. Appl. Math.*, vol. 68, no. 4, pp. 925–946, Jan. 2008.
[27] J. Shi and S. Osher, ''A nonlinear inverse scale space method for a convex multiplicative noise model,'' *SIAM J. Imag. Sci.*, vol. 1, no. 3, pp. 294–321, Jan. 2008.
[28] Y.-M. Huang, M. K. Ng, and Y.-W. Wen, ''A new total variation method for multiplicative noise removal,'' *SIAM J. Imag. Sci.*, vol. 2, no. 1, pp. 20–40, Jan. 2009.
[29] G. Steidl and T. Teuber, ''Removing multiplicative noise by douglas-rachford splitting methods,'' *J. Math. Imag. Vis.*, vol. 36, no. 2, pp. 168–184, Dec. 2009.
[30] F. Dong, H. Zhang, and D.-X. Kong, ''Nonlocal total variation models for multiplicative noise removal using split Bregman iteration,'' *Math. Comput. Model.*, vol. 55, nos. 3–4, pp. 939–954, Feb. 2012.
[31] D.-Q. Chen and L.-Z. Cheng, ''Spatially adapted total variation model to remove multiplicative noise,'' *IEEE Trans. Image Process.*, vol. 21, no. 4, pp. 1650–1662, Apr. 2012.
[32] Y.-M. Huang, L. Moisan, M. K. Ng, and T. Zeng, ''Multiplicative noise removal via a learned dictionary,'' *IEEE Trans. Image Process.*, vol. 21, no. 11, pp. 4534–4543, Nov. 2012.
[33] L. Jacques, L. Duval, C. Chaux, and G. Peyré, ''A panorama on multiscale geometric representations, intertwining spatial, directional and frequency selectivity,'' *Signal Process.*, vol. 91, no. 12, pp. 2699–2730, Dec. 2011.
[34] Q. Wang, J. Tan, T. Xing, F. Chen, and J. Niu, ''SID: Sensor-Assisted Image Deblurring System for Mobile Devices,'' *IEEE Access*, vol. 7, pp. 146607–146619, 2019.

[35] F. Li, M. K. Ng, and C. Shen, "Multiplicative noise removal with spatially varying regularization parameters," *SIAM J. Imag. Sci.*, vol. 3, no. 1, pp. 1–20, Jan. 2010.
[36] F. Wang, X.-L. Zhao, and M. K. Ng, "Multiplicative noise and blur removal by framelet decomposition and ℓ_1-based L-curve method," *IEEE Trans. Image Process.*, vol. 25, no. 9, pp. 4222–4232, Jun. 2016.
[37] L. Chen, F. Fang, T. Wang, and G. Zhang, "Blind image deblurring with local maximum gradient prior," in *Proc. IEEE/CVF Conf. Comput. Vis. Pattern Recognit. (CVPR)*, Jun. 2019, pp. 1742–1750.
[38] Y.-M. Huang, H.-Y. Yan, and T. Zeng, "Multiplicative noise removal based on unbiased box-cox transformation," *Commun. Comput. Phys.*, vol. 22, no. 3, pp. 803–828, Jul. 2017.
[39] T. Wu, D. Z. W. Wang, Z. Jin, and J. Zhang, "Solving constrained TV2L1-L2 MRI signal reconstruction via an efficient alternating direction method of multipliers," *Numer. Math., Theory, Methods Appl.*, vol. 10, no. 4, pp. 895–912, Sep. 2017.
[40] Y. Dong and T. Zeng, "A convex variational model for restoring blurred images with multiplicative noise," *SIAM J. Imag. Sci.*, vol. 6, no. 3, pp. 1598–1625, Jan. 2013.
[41] F. Wang and M. K. Ng, "A fast minimization method for blur and multiplicative noise removal," *Int. J. Comput. Math.*, vol. 90, no. 1, pp. 48–61, Jan. 2013.
[42] Y. Dong and T. Zeng, "New hybrid variational recovery model for blurred images with multiplicative noise," *East Asian J. Appl. Math.*, vol. 3, no. 4, pp. 263–282, May 2015.
[43] X.-L. Zhao, F. Wang, and M. K. Ng, "A new convex optimization model for multiplicative noise and blur removal," *SIAM J. Imag. Sci.*, vol. 7, no. 1, pp. 456–475, Jan. 2014.
[44] M.-G. Shama, T.-Z. Huang, J. Liu, and S. Wang, "A convex total generalized variation regularized model for multiplicative noise and blur removal," *Appl. Math. Comput.*, vol. 276, pp. 109–121, Mar. 2016.
[45] J. Liu, M. Yan, and T. Zeng, "Surface-aware blind image deblurring," *IEEE Trans. Pattern Anal. Mach. Intell.*, to be published.
[46] A. Ullah, W. Chen, M. A. Khan, and H. Sun, "A new variational approach for multiplicative noise and blur removal," *PLoS ONE*, vol. 12, no. 1, Jan. 2017, Art. no. e0161787.
[47] L. Zhong, S. Cho, D. Metaxas, S. Paris, and J. Wang, "Handling noise in single image deblurring using directional filters," in *Proc. IEEE Conf. Comput. Vis. Pattern Recognit.*, Jun. 2013, pp. 612–619.
[48] S. Xie, X. Zheng, W.-Z. Shao, Y.-D. Zhang, T. Lv, and H. Li, "Non-blind image deblurring method by the total variation deep network," *IEEE Access*, vol. 7, pp. 37536–37544, 2019.
[49] J.-F. Cai, H. Ji, C. Liu, and Z. Shen, "Blind motion deblurring from a single image using sparse approximation," in *Proc. IEEE Conf. Comput. Vis. Pattern Recognit.*, Jun. 2009, pp. 104–111.
[50] J. Lu, Z. Yang, L. Shen, Z. Lu, H. Yang, and C. Xu, "A framelet algorithm for de-blurring images corrupted by multiplicative noise," *Appl. Math. Model.*, vol. 62, pp. 51–61, Oct. 2018.
[51] T. Wu, W. Zhang, D. Z. W. Wang, and Y. Sun, "An efficient Peaceman–Rachford splitting method for constrained TGV-shearlet-based MRI reconstruction," *Inverse Problems Sci. Eng.*, vol. 27, no. 1, pp. 115–133, Mar. 2018.
[52] T. Wu and J. Shao, "Nonconvex and convex coupling image segmentation via TGPV regularization and thresholding," *Adv. Appl. Math. Mech.*, to be published.
[53] B. Münch, P. Trtik, F. Marone, and M. Stampanoni, "Stripe and ring artifact removal with combined wavelet—Fourier filtering," *Opt. Express*, vol. 17, no. 10, p. 8567, May 2009.
[54] F. E. Boas and D. Fleischmann, "CT artifacts: Causes and reduction techniques," *Imag. Med.*, vol. 4, no. 2, pp. 229–240, Apr. 2012.
[55] J. Henrik Fitschen, J. Ma, and S. Schuff, "Removal of curtaining effects by a variational model with directional forward differences," 2015, *arXiv:1507.00112*. [Online]. Available: http://arxiv.org/abs/1507.00112
[56] J. Roels, J. Aelterman, J. De Vylder, H. Luong, Y. Saeys, S. Lippens, and W. Philips, "Noise analysis and removal in 3D electron microscopy," in *Proc. Int. Symp. Vis. Comput.* Cham, Switzerland: Springer, 2014, pp. 31–40.
[57] Y. Chen, T.-Z. Huang, X.-L. Zhao, L.-J. Deng, and J. Huang, "Stripe noise removal of remote sensing images by total variation regularization and group sparsity constraint," *Remote Sens.*, vol. 9, no. 6, p. 559, Jun. 2017.
[58] P. Han, F. Dong, K. Jia, and B. Han, "PolSAR image speckle reduction based on classification of similarity features between coherency matrices," *IEEE Access*, vol. 7, pp. 136986–136994, 2019.
[59] J.-H. Yang, X.-L. Zhao, T.-H. Ma, Y. Chen, T.-Z. Huang, and M. Ding, "Remote sensing images destriping using unidirectional hybrid total variation and nonconvex low-rank regularization," *J. Comput. Appl. Math.*, vol. 363, pp. 124–144, Jan. 2020.
[60] L. I. Rudin, S. Osher, and E. Fatemi, "Nonlinear total variation based noise removal algorithms," *Phys. D, Nonlinear Phenomena*, vol. 60, nos. 1–4, pp. 259–268, Nov. 1992.
[61] M. Bertero, P. Boccacci, G. Talenti, R. Zanella, and L. Zanni, "A discrepancy principle for Poisson data," *Inverse Problems*, vol. 26, no. 10, Aug. 2010, Art. no. 105004.
[62] Z. Wang, A. C. Bovik, H. R. Sheikh, and E. P. Simoncelli, "Image quality assessment: From error visibility to structural similarity," *IEEE Trans. Image Process.*, vol. 13, no. 4, pp. 600–612, Apr. 2004.
[63] G.-H. Chen, C.-L. Yang, L.-M. Po, and S.-L. Xie, "Edge-based structural similarity for image quality assessment," in *Proc. IEEE Int. Conf. Acoust. Speech Signal Process.*, vol. 2, May 2006, p. 2.
[64] M. S. Hosseini and K. N. Plataniotis, "Convolutional deblurring for natural imaging," *IEEE Trans. Image Process.*, vol. 29, pp. 250–264, Jul. 2020.
[65] A. E. Savakis and H. J. Trussell, "Blur identification by residual spectral matching," *IEEE Trans. Image Process.*, vol. 2, no. 2, pp. 141–151, Apr. 1993.
[66] A. Levin, Y. Weiss, F. Durand, and W. T. Freeman, "Understanding blind deconvolution algorithms," *IEEE Trans. Pattern Anal. Mach. Intell.*, vol. 33, no. 12, pp. 2354–2367, Dec. 2011.

TINGTING WU received the B.S. and Ph.D. degrees in mathematics from Hunan University, Changsha, China, in 2006 and 2011, respectively. From 2015 to 2018, she was a Postdoctoral Researcher with the School of Mathematical Sciences, Nanjing Normal University, Nanjing, China. From 2016 to 2017, she was a Research Fellow with Nanyang Technological University, Singapore. She is currently an Associate Professor with the School of Science, Nanjing University of Posts and Telecommunications, Nanjing. Her research interests include variational methods for image processing and computer vision, optimization methods and their applications in sparse recovery, and regularized inverse problems.

WEI LI received the B.S. degree in statistics from the Anhui University of Finance and Economics, Bengbu, China, in 2018. He is currently pursuing the M.S. degree with the School of Science, Nanjing University of Posts and Telecommunications, Nanjing, China. His research interests include image processing and machine learning.

LIHUA LI received the B.S. degree from Xidian University, Xi'an, China, in 1985, and the Ph.D. degree from Southeast University, Nanjing, China, in 1990. He is currently a Professor with the College of Life Information Science and Instrument Engineering, Hangzhou Dianzi University, Hangzhou, China. His research interests include biomedical science and intelligent diagnosis.

TIEYONG ZENG received the B.S. degree from Peking University, Beijing, China, in 2000, the M.S. degree from École Polytechnique, Palaiseau, France, in 2004, and the Ph.D. degree from the University of Paris XIII, Paris, France,, in 2007. He is currently an Associate Professor with the Department of Mathematics, The Chinese University of Hong Kong. His research interests include image processing, optimization, artificial intelligence, scientific computing, computer vision, machine learning, and inverse problems.